Generalized Algebraic Algorithm for Scene-based Nonuniformity Correction

Majeed M. Hayat[a]*, Bradley M. Ratliff[a], J. Scott Tyo[a] and Kamil Agi[b]

[a]University of New Mexico, Department of Electrical and Computer Engineering, Albuquerque, NM, USA 87131
[b]K & A Wireless LLC, 2617 Juan Tabo, NE., Suite A, Albuquerque, NM, USA 87112

ABSTRACT

This paper presents an overview of three recently developed scene-based nonuniformity correction techniques, namely, the algebraic scene-based algorithm (ASBA), the extended radiometrically accurate scene-based algorithm (RASBA) and the generalized algebraic scene-based algorithm (GASBA). The ASBA uses pairs of image frames that exhibit one-dimension sub-pixel motion to algebraically extract estimates of bias nonuniformity. The RASBA incorporates arbitrary sub- and super-pixel two-dimensional motion in conjunction with limited perimeter-only absolute calibration to obtain radiometrically accurate estimates of the bias nonuniformity. The RASBA provides the advantage of being able to maintain radiometry in the interior photodetectors without interrupting their operation. The GASBA is a generalized non-radiometric form of the algorithm that uses image pairs with arbitrary two-dimensional motion and encompasses both the ASBA and RASBA algorithms. This generalization is accomplished by initially guaranteeing bias uniformity in the perimeter detectors. This uniformity can be achieved by first applying the ASBA estimates. The generalized algorithm is then able to automatically maintain perimeter uniformity without the need for re-application of the ASBA. Thus, the GASBA is able to operate completely in a non-radiometric mode, alleviating the need for the perimeter calibration system if desired. The generalized algorithm is applied to real infrared imagery obtained from both cooled and uncooled infrared cameras. A hardware implementation of the proposed algorithm will also be discussed along with several ongoing commercial applications of the technology.

Keywords: focal plane array, nonuniformity correction, scene-based NUC, fixed pattern noise, infrared sensors, calibration

1. INTRODUCTION

Focal-plane array (FPA) sensors have become the most prominent detector used in infrared (IR) and visible-light imaging systems in recent years. The wide usage of FPAs is primarily attributable to advances in solid-state detector technology that has lead to compactness, cost-effective production and high performance.[1] One of the primary applications of long-wave infrared (LWIR) and mid-wave infrared (MWIR) sensor arrays is broadband thermal imaging, where maximizing broadband spatial resolution and intensity signal-to-noise ratio is of paramount importance. A few applications include night-vision systems, airborne and space-based reconnaissance and surveillance systems, astronomical imaging, and forest-fire early detection systems.

IR FPA sensors all suffer from a common problem known as fixed pattern noise (FPN), or spatial nonuniformity.[1] In fact, FPN remains a serious problem despite recent advances in IR FPA technology.[2] The source of this FPN is attributed to the fact that each photodetector in the FPA has a differing photoresponse due to detector-to-detector variability in the FPA fabrication process.[3] Simply stated, each detector in the array will respond differently to the same amount of impinging radiation. FPN is so termed because it manifests as a spatially-random, temporally-constant pattern that is present across all frames of motion.

At first glance, it would appear that the FPN problem could be remedied through a one-time factory calibration. But, the problem is complicated by the fact that the response of each FPA photodetector changes in time, causing the FPN to slowly drift throughout sensor operation, e.g., due to factors such as the sensor operating

*E-mail: hayat@ece.unm.edu, Telephone: 1 505 277-0297

temperature, the temperature of the observed scene, the FPA fabrication material, electronic readout noise, etc. Thus, a one-time calibration is ineffective and instead a solution is required that continuously estimates and compensates for the FPN throughout camera operation. Though the true response of each FPA detector is nonlinear, the response is typically modelled linearly, having both a gain and bias component. Thus, under this linear assumption, the gain and bias are different for each detector and hence give rise to the nonuniformity. Techniques that seek to estimate these gain and bias parameters, and subsequently employ the estimates to remove the nonuniformity, are known as nonuniformity correction (NUC) techniques.

NUC techniques fall into two main categories, namely, calibration-based and scene-based techniques. Calibration-based methods employ some form of absolute temperature reference, such as a blackbody radiation source or a uniform-temperature shutter, to estimate the FPN. The calibration is performed by heating the source to a uniform, known temperature and placing it within the full camera field of view (FOV). The resulting "flat" images can then be used to linearly extract the nonuniformity. A standard form of calibration is the two-point calibration (TPC), and is so called because the source is imaged at two distinct temperatures. From these two spatially-uniform image sequences the gain and bias parameters can be directly extracted. When only the bias parameters are desired a single uniform-temperature sequence (called a one-point calibration) may be employed. Similarly, to more accurately characterize the nonlinear behavior of the detector response, a multi-point calibration can be used to obtain a higher-order estimate of each detector response curve.[4]

Calibration-based techniques have the desirable property that they provide reasonably good estimates of the nonuniformity, and, after correction, the resulting imagery is radiometrically accurate. The main disadvantage of these techniques is that, due to drift in the FPN, the FPA must be recalibrated on the order of minutes throughout camera operation. Thus, the camera is "blind" during these periods. Furthermore, because the calibration procedure itself can take a reasonable amount of time, e.g., several minutes in the TPC, most real-time imaging systems are forced to use the less accurate one-point calibration procedure. In addition, it may be undesirable to endure the expense of the blackbody source, particularly for applications where radiometry is of no concern.

The alternative to these obstructive calibration-based procedures are scene-based NUC techniques. These techniques are algorithmic by nature and provide the advantage of being non-obstructive at the cost of compromising radiometric accuracy. Scene-based algorithms are generally identified by two main approaches, namely, statistical and image registration-based. Statistical techniques generally make some spacio-temporal assumptions on the irradiance observed by each detector in the array and exploit these assumptions to extract quantities used to compensate for the FPN. Registration-based techniques, on the other hand, require the precise estimation of frame-to-frame translational motion that is then used to "line up," or register, all image frames within the sequence. Then, after image alignment, specific assumptions are introduced and the nonuniformity compensators are estimated.

Statistical algorithms have been reported by Narendra and Foss,[5,6] Harris and Chiang,[7,8] and Chiang and Harris.[9] These algorithms rely on the constant-statistic assumption, which states that the statistics of the observed scene become constant over time. Thus, this assumption requires that each detector in the array spend a reasonable amount of time observing a wide range of irradiance values. Under this assumption and by employing a linear model for the detector response, the mean and standard deviation of each detector's readout signal can be regarded as its bias and gain, respectively. A statistical algorithm developed by Hayat *et al.*[10] relaxes the constant-statistic assumption to one that relies on the key assumption that, in time, all detectors in the array are exposed to the same range of irradiance. A Kalman-filtering approach was recently presented by Torres and Hayat[11,12] that adopts the constant-range assumption and is able to capture stochastic drift in the nonuniformity parameters. Scribner *et al.*[13] proposed a least mean square error technique that resembles adaptive temporal high-pass filtering. By adjusting the time constant of the filter, their algorithm was used to reduce the spatial noise caused by bias nonuniformity. A neural-network implementation of the adaptive least mean square error algorithm was also developed by Scribner *et al.*[14,15]

Typically, statistical algorithms perform poorly when the imposed assumptions are violated. Moreover, many of these techniques typically require thousands of image frames in order to obtain reasonable NUC, depending on the spatial distribution of the scene and the level of motion.

Registration-based techniques include those developed by O'Neil,[16,17] Hardie, *et al.*[18] and Hepfer *et al.*[19] These techniques all use the idea that each detector should have an identical response when observing the same scene point over time. For example, O'Neil uses image frames produced by dithering the detector FOV between consecutive frames in a known pattern. In contrast, the technique developed by Hardie *et al.* uses a motion-estimation algorithm to trace each point in the scene across all image frames. In general, registration-based algorithms offer a faster nonuniformity-estimate convergence rate, e.g., on the order of hundreds of frames, than statistical NUC algorithms at the cost of an increase in computational complexity due to their need for motion estimation or induced motion.

We now focus on a class of registration-based algorithms recently developed by Ratliff *et al.*[20–24] The algebraic scene-based algorithm (ASBA)[20,21] uses image pairs that exhibit subpixel one-dimensional (1D) translational motion, or shift, to unify the detector biases across the entire array to that of a single common bias value. The technique was later extended by the authors to a radiometrically accurate form (RASBA) that accommodates arbitrary, sub- or super-pixel two-dimensional (2D) global motion.[23,25] This extension was achieved by employing a limited perimeter-only blackbody calibration system that absolutely calibrates detectors along the perimeter of the FPA while leaving interior detectors unobstructed. The corrected imagery resulting from this technique is radiometrically accurate in a sense that all of the pixels – not just the calibrated perimeter pixels – have zero bias. The RASBA technique enjoys the non-obstructive advantage of scene-based algorithms while yielding the radiometric benefit of calibration techniques. Later, it was observed that the algorithm could further be generalized to a form capable of utilizing arbitrary two-dimensional image pairs without the need for the perimeter calibration system. This extension was achieved by (1) unifying the bias values of detectors along the perimeter to a single unknown bias value through application of the ASBA; and (2) once perimeter uniformity has been accomplished, a new version of the RASBA algorithm is applied which *does not* require calibration of the perimeter detectors. Thus, in applications where absolute radiometric accuracy is not necessary, this generalized algebraic scene-based algorithm (GASBA)[24] allows for removal of the nonuniformity in practically all cases where a video sequence is available with global translational motion. Consequently and more importantly, the performance of the GASBA is significantly better than that of the ASBA technique, removing image artifacts such as horizontal or vertical striping that were observed in the original ASBA corrections.

This paper is structured as follows. Section 2 presents the linear relationships used to model each photodetector response within the FPA along with a bilinear model used to estimate each shifted irradiance value. In Section 3, brief reviews of the ASBA, RASBA and GASBA NUC techniques are presented. The NUC algorithms are applied to real infrared data obtained from both cryogenically-cooled and uncooled infrared FPAs in Section 4. Finally, conclusions are stated in Section 5.

2. DETECTOR MODELS

Consider an image sequence y_k generated by an $M \times N$ FPA, where $k = 1, 2, 3, \ldots$ represents the image frame number. A commonly used linear model for the ijth FPA-sensor output at time k is given by

$$y_k(i,j) = z_k(i,j) + b(i,j), \tag{1}$$

where $z_k(i,j)$, here termed the irradiance, is proportional to the number of photons collected by the ijth detector during the camera integration time, $b(i,j)$ is the detector bias, $i = 1, 2, \ldots, M$ and $j = 1, 2, \ldots, N$.

We assume throughout that the temperature of objects does not change significantly during the time between image frames. Thus, when two image frames exhibit an arbitrary translational motion between them, we approximate the irradiance at a given pixel in the $(k+1)$th frame as a bilinear interpolation of the irradiance corresponding to the appropriate four pixels from the kth frame. This is done as follows: Let α_k and β_k be the vertical and horizontal components of the shift between the kth and the $(k+1)$th images, respectively. Further, let us write these shifts as the sum of their whole-integer and fractional parts, i.e., $\alpha_k = \lfloor \alpha_k \rfloor + \Delta\alpha_k$ and $\beta_k = \lfloor \beta_k \rfloor + \Delta\beta_k$, where $\lfloor \cdot \rfloor$ indicates the integer part of the shift. For convenience, we define the fractional areas $\gamma_{1,k} = |\Delta\alpha_k \Delta\beta_k|$, $\gamma_{2,k} = (1 - |\Delta\alpha_k|)|\Delta\beta_k|$, $\gamma_{3,k} = |\Delta\alpha_k|(1 - |\Delta\beta_k|)$, and $\gamma_{4,k} = (1 - |\Delta\alpha_k|)(1 - |\Delta\beta_k|)$. Note that $\gamma_{1,k} + \gamma_{2,k} + \gamma_{3,k} + \gamma_{4,k} = 1$. For simplicity, we assume that the shift is in the down-rightward direction and

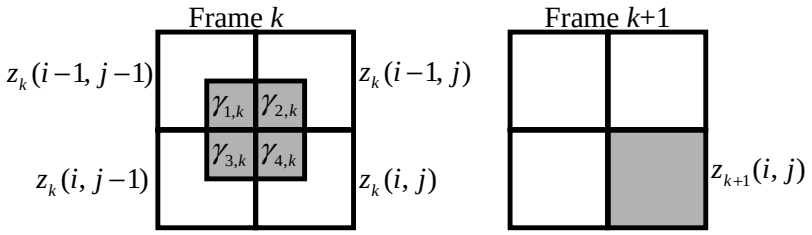

Figure 1. Graphical depiction of the bilinear irradiance interpolation model for the case of subpixel 2D motion. The pixels shaded in blue represent the interpolated IR-signal value at time $k+1$.

thus by convention $\alpha_k > 0$ and $\beta_k > 0$. With this simplifying notation, the bilinear-interpolation approximation $\hat{z}_{k+1}(i,j)$ for the irradiance $z_{k+1}(i,j)$ becomes

$$\begin{aligned}\hat{z}_{k+1}(i,j) &= \gamma_{1,k} z_k(i - \lfloor \alpha_k \rfloor - 1, j - \lfloor \beta_k \rfloor - 1) + \gamma_{2,k} z_k(i - \lfloor \alpha_k \rfloor, j - \lfloor \beta_k \rfloor - 1) \\ &\quad + \gamma_{3,k} z_k(i - \lfloor \alpha_k \rfloor - 1, j - \lfloor \beta_k \rfloor) + \gamma_{4,k} z_k(i - \lfloor \alpha_k \rfloor, j - \lfloor \beta_k \rfloor). \end{aligned} \tag{2}$$

This irradiance interpolation model is depicted graphically in Fig. 1. By substituting the above interpolation model into Eq. 1, we obtain a bilinearly-interpolated approximation for the $(k+1)$th detector output in terms of the irradiance's spatial distribution in the previous frame. More precisely, for $i = 2 + \lfloor \alpha_k \rfloor, 3 + \lfloor \alpha_k \rfloor, \ldots, M$ and $j = 2 + \lfloor \beta_k \rfloor, 3 + \lfloor \beta_k \rfloor, \ldots, N$,

$$\begin{aligned}y_{k+1}(i,j) &= \gamma_{1,k} z_k(i - \lfloor \alpha_k \rfloor - 1, j - \lfloor \beta_k \rfloor - 1) + \gamma_{2,k} z_k(i - \lfloor \alpha_k \rfloor, j - \lfloor \beta_k \rfloor - 1) \\ &\quad + \gamma_{3,k} z_k(i - \lfloor \alpha_k \rfloor - 1, j - \lfloor \beta_k \rfloor) + \gamma_{4,k} z_k(i - \lfloor \alpha_k \rfloor, j - \lfloor \beta_k \rfloor) + b(i,j). \end{aligned} \tag{3}$$

Having established the above detector response models, we next review the key aspects behind the three NUC techniques.

3. ALGORITHM DESCRIPTIONS

We next present a brief review of all relevant mathematics behind the ASBA, RASBA and GASBA NUC techniques.

3.1. Review of the ASBA NUC Technique

We begin by reviewing the key ideas behind the original ASBA NUC technique.[21] This review illustrates the fundamental concepts behind the bias unification ability of the various algorithms. The ASBA technique exploits shift information between two consecutive image frames, exhibiting a purely vertical shift, say, to convert the bias value in a given detector element to the bias value of its vertical neighbor. This mechanism, in turn, allows for the conversion of all detector biases in an entire column to a common bias value. The procedure is repeated for every column in the image pair, resulting in an image that suffers from nonuniformity across rows only, i.e., each column has a different, yet uniform, bias value. Now, with an analogous procedure and by using a pair of horizontally-shifted images, the bias values are unified across all rows, ultimately allowing for the unification of all biases in the array to a common value.

To precisely describe the ASBA procedure, we first define $\mathcal{V}$ as the set containing P image pairs exhibiting 1D subpixel vertical motion. Similarly, $\mathcal{H}$ denotes the set of Q 1D subpixel horizontally-shifted image pairs. We then define an intermediate vertical correction matrix $\Delta_{V,p}$ for a pair of vertically-shifted frames at times p and $p+1$. For $j = 1, 2, \ldots, N$, put $\Delta_{V,p}(1,j) = 0$, and for $i = 2, 3, \ldots, M$, define

$$\begin{aligned}\Delta_{V,p}(i,j) &= \frac{1}{|\Delta\alpha_p|}\big[|\Delta\alpha_p| y_p(i-1,j) + (1 - |\Delta\alpha_p|) y_p(i,j) - y_{p+1}(i,j)\big] \\ &= b(i-1,j) - b(i,j). \end{aligned} \tag{4}$$

Hence

$$\Delta_{V,p} = \begin{bmatrix} 0 & 0 & \cdots & 0 \\ b(1,1)-b(2,1) & b(1,2)-b(2,2) & \cdots & b(1,N)-b(2,N) \\ b(2,1)-b(3,1) & b(2,2)-b(3,2) & \cdots & b(2,N)-b(3,N) \\ \vdots & \vdots & \ddots & \vdots \\ b(M-1,1)-b(M,1) & b(M-1,2)-b(M,2) & \cdots & b(M-1,N)-b(M,N) \end{bmatrix}. \tag{5}$$

Now, the vertical correction matrix $\mathbf{C}_{V,p}$ is calculated by performing a partial cumulative sum down each column of $\Delta_{V,p}$. So, for $i = 2, 3, \ldots, M$ and $j = 1, 2, \ldots, N$, we define

$$\mathbf{C}_{V,p}(i,j) \quad = \quad \sum_{m=2}^{i} \Delta_{V,p}(m,j) = b(1,j) - b(i,j), \tag{6}$$

so that

$$\mathbf{C}_{V,p} = \begin{bmatrix} 0 & 0 & \cdots & 0 \\ b(1,1)-b(2,1) & b(1,2)-b(2,2) & \cdots & b(1,N)-b(2,N) \\ b(1,1)-b(3,1) & b(1,2)-b(3,2) & \cdots & b(1,N)-b(3,N) \\ \vdots & \vdots & \ddots & \vdots \\ b(1,1)-b(M,1) & b(1,2)-b(M,2) & \cdots & b(1,N)-b(M,N) \end{bmatrix}. \tag{7}$$

Thus, the top-most bias value for each column has been propagated into all correction values within its respective column. Now, because vertical correction matrices are computed for all image pairs in $\mathcal{V}$, each $\mathbf{C}_{V,p}$ may be averaged in time to reduce the effects of estimation error (the sources of this error are studied extensively in Ref. 24). Thus, each element of the averaged vertical correction matrix $\mathbf{C}_V$ is given by

$$\mathbf{C}_V(i,j) \quad = \quad \frac{1}{P} \sum_{p \in \mathcal{V}} \mathbf{C}_{V,p}(i,j) = \bar{b}(1,j) - \bar{b}(i,j), \tag{8}$$

Next, we apply $\mathbf{C}_V$ to each image pair in $\mathcal{H}$, resulting in the vertically corrected set of horizontally-shifted image pairs $\mathcal{H}^V$. Then, a similar bias unification procedure is performed for an image pair from $\mathcal{H}^V$, at times q and $q+1$, to obtain the horizontal matrix $\Delta_{H,q}$, i.e., for $i = 1, 2, \ldots, M$ and $j = 2, 3, \ldots, N$, put $\Delta_{H,q}(i,1) = 0$ and

$$\Delta_{H,q}(i,j) \quad = \quad \frac{1}{|\Delta\beta_q|}\big[|\Delta\beta_q| y_q^V(i,j-1) + (1-|\Delta\beta_q|) y_q^V(i,j) - y_{q+1}^V(i,j)\big], \tag{9}$$

where y_q^V denotes a vertically-corrected image frame from $\mathcal{H}^V$. Performing a partial cumulative sum across each row of $\Delta_{H,q}$, the horizonal correction matrix is

$$\mathbf{C}_{H,q} = \begin{bmatrix} 0 & \bar{b}(1,1)-\bar{b}(1,2) & \bar{b}(1,1)-\bar{b}(1,3) & \cdots & \bar{b}(1,1)-\bar{b}(1,N) \\ 0 & \bar{b}(1,1)-\bar{b}(1,2) & \bar{b}(1,1)-\bar{b}(1,3) & \cdots & \bar{b}(1,1)-\bar{b}(1,N) \\ \vdots & \vdots & \vdots & \ddots & \vdots \\ 0 & \bar{b}(1,1)-\bar{b}(1,2) & \bar{b}(1,1)-\bar{b}(1,3) & \cdots & \bar{b}(1,1)-\bar{b}(1,N) \end{bmatrix}. \tag{10}$$

Notice that because the horizontal correction matrix was computed for each vertically-corrected image pair in $\mathcal{H}^V$, each row of the above horizontal correction matrix is identical. Similar to the vertical case, the horizontal correction matrices are computed for all image pairs in $\mathcal{H}^V$, and hence are averaged in time. Thus, each element of the averaged horizontal correction matrix $\mathbf{C}_H$ is given by

$$\mathbf{C}_H(i,j) \quad = \quad \frac{1}{Q} \sum_{q \in \mathcal{H}^V} \mathbf{C}_{H,q}(i,j). \tag{11}$$

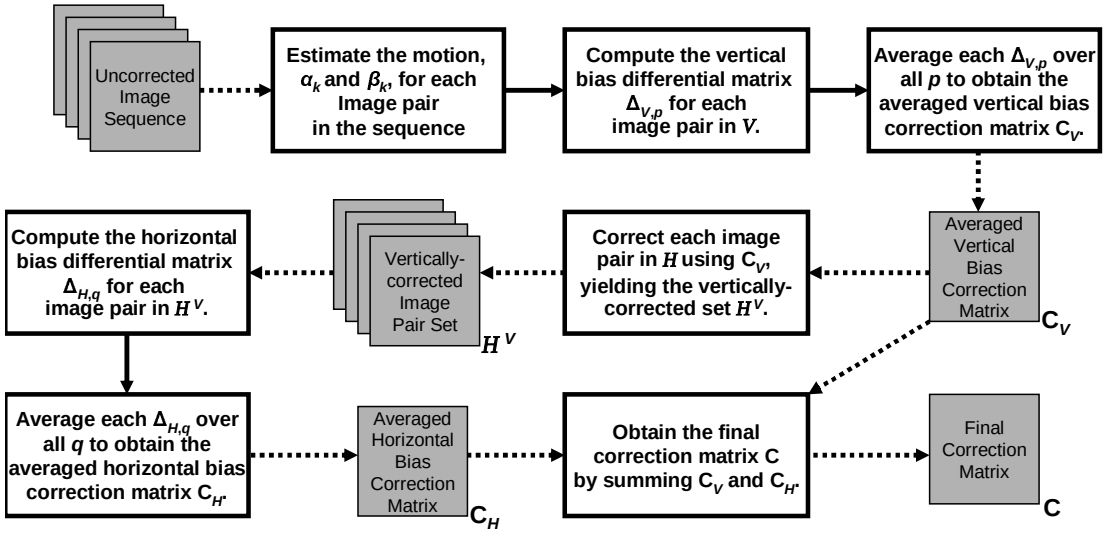

Figure 2. Diagram illustrating the steps involved in the ASBA technique to compute the final correction matrix $\mathbf{C}$.

Having obtained both vertical and horizontal correction matrices, we form the total correction matrix $\mathbf{C}$ simply by summing $\mathbf{C}_V$ and $\mathbf{C}_H$, i.e.,

$$\mathbf{C} = \mathbf{C}_V + \mathbf{C}_H = \begin{bmatrix} 0 & \bar{\bar{b}}(1,1) - \bar{\bar{b}}(1,2) & \cdots & \bar{\bar{b}}(1,1) - \bar{\bar{b}}(1,N) \\ \bar{\bar{b}}(1,1) - \bar{\bar{b}}(2,1) & \bar{\bar{b}}(1,1) - \bar{\bar{b}}(2,2) & \cdots & \bar{\bar{b}}(1,1) - \bar{\bar{b}}(2,N) \\ \vdots & \vdots & \ddots & \vdots \\ \bar{\bar{b}}(1,1) - \bar{\bar{b}}(M,1) & \bar{\bar{b}}(1,1) - \bar{\bar{b}}(M,2) & \cdots & \bar{\bar{b}}(1,1) - \bar{\bar{b}}(M,N) \end{bmatrix}. \tag{12}$$

Observe that the bias term $\bar{\bar{b}}(1,1)$ is common to each element of $\mathbf{C}$. Furthermore, notice that if C is added to an arbitrary raw image frame, each respective bias term will be removed and replaced by $\bar{\bar{b}}(1,1)$. Thus, after correction, every detector bias in the array is unified to the same, although unknown, bias value. A block diagram summarizing the key steps of the ASBA technique is shown in Fig. 2.

It is important to note that, in addition to its restrictive 1D subpixel nature, the ASBA technique produces nonuniformity correction estimates that tend to leave behind artifacts in the corrected imagery. These artifacts manifest as nonuniformity-like patterns that are present across rows and columns. Though subtle, these striping patterns are undesirable and motivate the need for an improvement to the existing ASBA technique. Two such improved algorithms are next presented that yield performance far superior to that of the original ASBA technique.

3.2. Review of the RASBA NUC Technique

The ASBA NUC technique cannot be directly extended to incorporate shifts outside the sub-pixel 1D domain. Instead, for this generalization to be accomplished, we discovered that a set of initial conditions are required. These boundary conditions were found to be knowledge of the nonuniformity along the perimeter of the FPA. To obtain these perimeter nonuniformity values, we employ a form of limited calibration only to detectors along the perimeter of the FPA.[23] Once these perimeter nonuniformity values are known, the algorithm can indeed be extended to the desired form with the ability to accommodate arbitrary translational motion. In addition to being able to accommodate more image pairs from the sequence, this form of the algorithm also provides the added benefit that the resulting corrected imagery within the non-perimeter detectors is radiometrically accurate. Thus, the algorithm provides a means for calibrating the interior of the FPA without ever obstructing the photodetectors with a calibration source. We next review the relevant aspects of the RASBA NUC technique. For a more thorough discussion we refer the reader to our earlier work.[23]

The maximum translational shift between consecutive image frames that can be used by the RASBA algorithm is set to the width of the calibrated perimeter, which is determined by the calibration system. This upper bound on the shift is denoted by L (pixels). We will assume henceforth that all image pairs satisfy the L-shift upper bound condition.

The key step in the RASBA technique is to compute the so-called bias differential $\Delta_k(i,j)$ for each non-perimeter detector. This bias differential is calculated from the image sequence as follows:[23]

$$\begin{aligned}\Delta_k(i,j) &= \gamma_{1,k}y_k(i-\lfloor\alpha_k\rfloor-1, j-\lfloor\beta_k\rfloor-1)+\gamma_{2,k}y_k(i-\lfloor\alpha_k\rfloor, j-\lfloor\beta_k\rfloor-1)\\ &\quad+\gamma_{3,k}y_k(i-\lfloor\alpha_k\rfloor-1, j-\lfloor\beta_k\rfloor)+\gamma_{4,k}y_k(i-\lfloor\alpha_k\rfloor, j-\lfloor\beta_k\rfloor)-y_{k+1}(i,j). \qquad (13)\end{aligned}$$

When we substitute Eqs. 1 and 3 into 13, we find that

$$\begin{aligned}\Delta_k(i,j) &= \gamma_{1,k}b(i-\lfloor\alpha_k\rfloor-1, j-\lfloor\beta_k\rfloor-1)+\gamma_{2,k}b(i-\lfloor\alpha_k\rfloor, j-\lfloor\beta_k\rfloor-1)\\ &\quad+\gamma_{3,k}b(i-\lfloor\alpha_k\rfloor-1, j-\lfloor\beta_k\rfloor)+\gamma_{4,k}b(i-\lfloor\alpha_k\rfloor, j-\lfloor\beta_k\rfloor)-b(i,j). \qquad (14)\end{aligned}$$

The bias-correction capability of the RASBA can now be described as follows. Suppose that we calibrate the top-most L rows and left-most L columns of detectors such that we force each perimeter detector to have a unity gain and zero bias. We then observe that for the top-leftmost uncalibrated detector, i.e., for $i = L+1$ and $j = L+1$, the differential bias $\Delta_k(L+1, L+1)$ is precisely equal to $-b(i,j)$ since all of the γ-scaled bias terms are equal to zero due to calibration. Hence, we define the first *bias compensator* corresponding to the kth frame pair as $c_k(L+1, L+1) = -\Delta_k(L+1, L+1)$. To compute the bias compensators in general, we must transform each $\Delta_k(i,j)$ term in Eq. 14 into the desired $-b(i,j)$ form. Thus, the (i,j)th bias compensator is obtained by progressively updating $\Delta_k(i,j)$ according to

$$\begin{aligned}c_k(i,j) &= \Delta_k(i,j)+\gamma_{1,k}c_k(i-\lfloor\alpha_k\rfloor-1, j-\lfloor\beta_k\rfloor-1)+\gamma_{2,k}c_k(i-\lfloor\alpha_k\rfloor, j-\lfloor\beta_k\rfloor-1)\\ &\quad+\gamma_{3,k}c_k(i-\lfloor\alpha_k\rfloor-1, j-\lfloor\beta_k\rfloor)+\gamma_{4,k}c_k(i-\lfloor\alpha_k\rfloor, j-\lfloor\beta_k\rfloor). \qquad (15)\end{aligned}$$

Clearly, the algorithm has a spatially-recursive structure. The recursion starts with the top-leftmost uncalibrated detector and proceeds in a down-rightward manner, updating one row or column of the bias differentials at a time. Each bias compensator is progressively estimated in this way until all array indexes have been exhausted. Notice that the calibrated detectors of the perimeter provide the necessary boundary conditions required to begin this recursive process. Finally, because the bias compensators are estimated for k image pairs, we average these k estimates for each (i,j)th detector to reduce the effects of estimation error.

We next review the generalized form of the algorithm that is capable of operating in a fully non-radiometric mode.

3.3. Review of the GASBA NUC Technique

Instead of using the perimeter calibration system to unify the L perimeter rows and columns, the ASBA technique is instead employed to perform an initial bias unification of the perimeter detectors. Thus, there is no longer a restriction to a fixed perimeter size, but instead the upper bound L is limited only by the accuracy of the shift estimator (for the shift estimation algorithm[26] we employed, $L = 30$ pixels). The perimeter size can now be dynamically selected for each image pair; therefore, for each image pair, we unify the biases of the topmost $\lfloor\alpha_k\rfloor + 1$ rows and left-most $\lfloor\beta_k\rfloor + 1$ columns. Next, given a 2D-shifted pair of perimeter-unified images, the RASBA algorithm is applied as described in Section 3.2.

To demonstrate that application of the RASBA will indeed unify all detectors in the FPA to a single bias value, we first compute the bias compensator for detector $(2+\lfloor\alpha_k\rfloor, 2+\lfloor\beta_k\rfloor)$. Notice that in this case the computation of the bias differential involves direct use of the perimeter detectors. Thus, the bias differential is

$$\Delta_k(2+\lfloor\alpha_k\rfloor, 2+\lfloor\beta_k\rfloor) = \gamma_{1,k}b+\gamma_{2,k}b+\gamma_{3,k}b+\gamma_{4,k}b-b(2+\lfloor\alpha_k\rfloor, 2+\lfloor\beta_k\rfloor). \qquad (16)$$

Since the γ terms sum to 1, Eq. 16 becomes

$$\Delta_k(2+\lfloor\alpha_k\rfloor, 2+\lfloor\beta_k\rfloor) = b-b(2+\lfloor\alpha_k\rfloor, 2+\lfloor\beta_k\rfloor). \qquad (17)$$

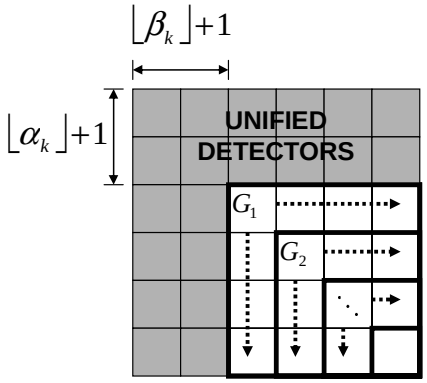

Figure 3. Graphical representation of the recursive operation of the algorithm. The unshaded pixel partitions correspond to each G_ℓ, representing the group of detectors whose biases are estimated iteratively in ℓ. The arrows indicate the direction of algorithm iteration within each G_ℓ.

Clearly, when this bias differential is added to the top-leftmost nonunified detector output $y(2+\lfloor\alpha_k\rfloor, 2+\lfloor\beta_k\rfloor)$, its bias is subtracted and replaced with a value of b, thus unifying this detector's bias to that of the perimeter. In this case, the bias differential is automatically of the desired form. In general, the bias differentials are of the form given in Eq. 14. To transform these bias differentials to the desired form of Eq. 17, a recursive update procedure similar to the RASBA is applied.

The GASBA technique is summarized below. A more thorough derivation of the technique is presented in Ref. 24. It is convenient to first partition the non-perimeter pixels as follows. For $\min(2+\lfloor\alpha_k\rfloor, 2+\lfloor\beta_k\rfloor) \le \ell \le \min(M,N)$, define G_ℓ to represent the group of pixels consisting of $\{(\ell,\ell),\ldots,(M,\ell),(\ell,\ell+1),\ldots,(\ell,N)\}$, as depicted in Fig. 3. Next, we organize all images in the sequence into pairs of adjacent image frames and denote each pair by I_k. Further, we define the image-pair set S_1 as the collection of all image pairs exhibiting subpixel 1D shifts, and the set S_2 as the collection of all image pairs exhibiting 2D sub- and superpixel shifts with the proviso that the maximum shift has an integral part no greater than L. Given these definitions, the GASBA is then summarized as follows:

1. Estimate the motion vector (α_k, β_k) for each I_k. Then, place each I_k in the appropriate group, namely, S_1 or S_2, according to its motion estimate.

2. *Initialization stage:* Extract the initial bias nonuniformity compensators by employing the ASBA technique in conjunction with the sequence S_1.

3. For each $I_k \in S_2$, unify the perimeter bias values, i.e., for $i = 1,\ldots,M, j = 1,\ldots,\lfloor\beta_k\rfloor+1$ and $i = 1,\ldots,\lfloor\alpha_k\rfloor+1, j = \lfloor\beta_k\rfloor+2,\ldots,N$, using the ASBA bias compensators calculated in the previous step. The perimeter thickness does not exceed L pixels.

4. *Lock-in stage:* For each k for which $I_k \in S_2$, compute the bias differentials $\Delta_k(i,j)$ in G_ℓ for all ℓ according to Eq. 13.

5. Update the bias differentials, resulting in the bias compensators $c_k(i,j)$ for each k using the following recursive procedure:

   (a) Start the recursion: Put $\ell = \min(2+\lfloor\alpha_k\rfloor, 2+\lfloor\beta_k\rfloor)$ and estimate the bias compensators in G_ℓ according to Eq. 15.

   (b) For each k for which $I_k \in S_2$, calculate the bias compensators $c_k(i,j)$ in $G_{\ell+1}$ according to Eq. 15 for $(i,j) \in G_{\ell+1}$.

   (c) Repeat the previous step and terminate the recursion when $\ell = 1+\min(M,N)$.

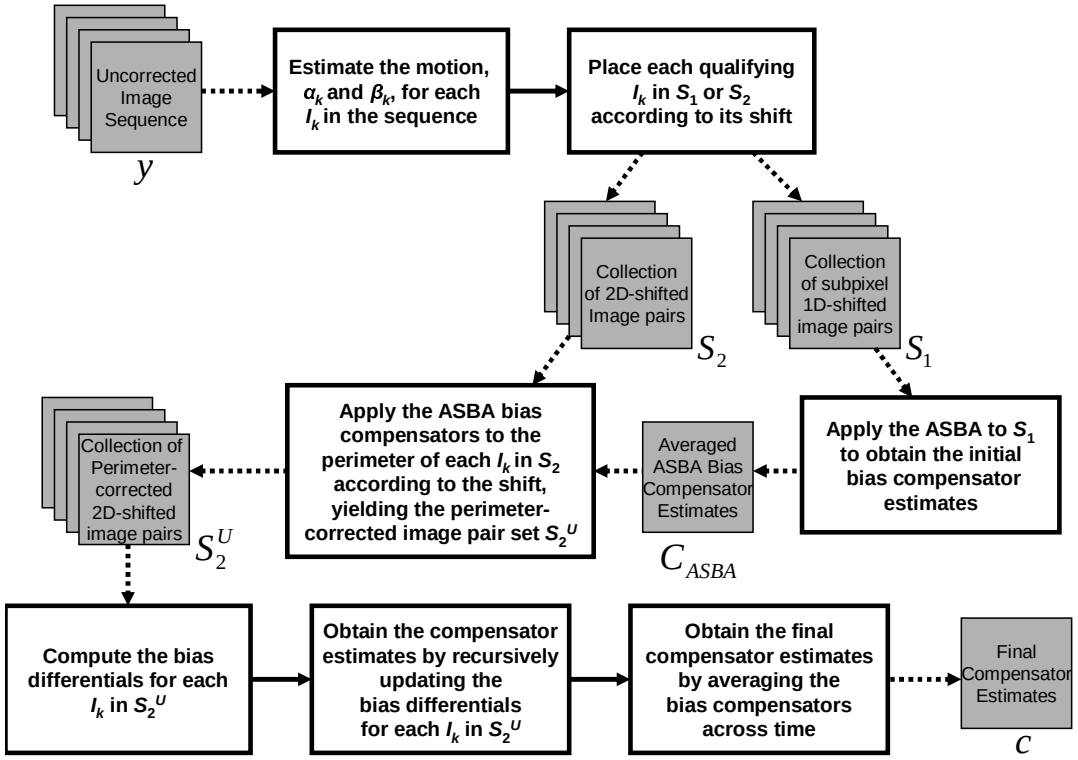

Figure 4. Diagram illustrating the steps involved in the GASBA technique.

6. Obtain the final bias compensators by computing the temporal average $c(i,j)$ of the bias compensator $c_k(i,j)$ over all image pairs I_k in S_2.

A block diagram illustrating the steps of the GASBA technique is shown in Fig. 4.

3.4. GASBA Real-time Hardware Implementation

The GASBA's high computational efficiency lends naturally to real-time applications. Currently, we are in process of implementing the GASBA algorithm into a real-time hardware environment. This task has required a redesign of the presented post-processing form of the algorithm. This new real-time processing structure has been fully simulated and validated in MATLAB. An initial implementation has been completed for simulation on a Texas Instruments Cx6000-based DSP board. The results of this simulation yielded more precise metrics on the algorithm's ability to operate in a real-time sense. It was found, using the current sub-optimum code, that a single iteration of the algorithm can be performed in approximately 68.4ms, corresponding to a frame rate of 14.6 frames/second. These metrics were assuming algorithm operation on a Texas Instruments Cx6711 DSP. It was also found that the algorithm code requires 27262 bytes of memory space, while the algorithm's data requirements are only 2MB of SDRAM (this is based upon an image size of 128x128). The overall MIPS requirement of the algorithm in its current un-optimized form is found to 68.25. We are confident that a full optimization of the code for the hardware platform will yield a dramatic improvement in the operating speed of the algorithm. Thus, it seems highly feasible that the algorithm will be able to achieve an entirely real-time capability as we continue this work.

4. ALGORITHM PERFORMANCE

In this section we employ real IR data to demonstrate the algorithms' ability to accurately remove the nonuniformity and study the number of estimates required to achieve good estimates of the bias compensators.

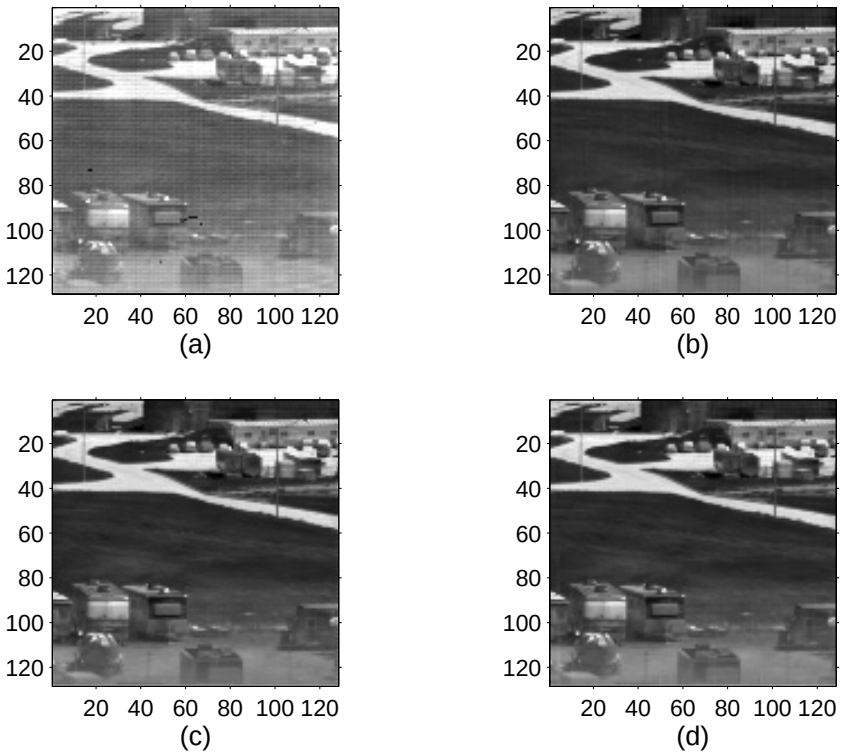

Figure 5. Image frame 325 from Data Set 1: (a) Raw image; (b) After correction by the ASBA; (c) After correction by the RASBA; (d) After correction by the GASBA. All images are statistically scaled to the same dynamic range.

4.1. Application to IR Data

The three algorithms were applied to real infrared data. Data Set 1 was collected using a cryogenically-cooled Amber 128x128 12-bit MWIR InSb camera. Figure 5.a shows the raw camera-outputted image frame 325 from this 512-frame image sequence. Notice the high degree of spatial nonuniformity present. The data sequence was then corrected using the ASBA, RASBA and GASBA techniques. The resulting images from these corrections are displayed in Figs. 5.b, 5.c and 5.d, respectively. Notice the residual vertical striping remaining in the ASBA image. This phenomena is typical of the ASBA and essentially results from all shifts being one dimensional, i.e., all corrections are performed strictly down rows and across columns. In the RASBA-corrected image, however, we notice that these artifacts are not present. In this case, the perimeter ($L = 5$) was unified through a two-point-calibration process, using flat images at 18° C and 30° C, to set all biases to zero and gains to unity. Consequently, the resulting imagery is radiometrically accurate.[23]

The GASBA-corrected image is also free of the striping artifacts. In the initialization stage of the GASBA, the bias nonuniformity estimates from the ASBA technique were first applied to the perimeter detectors. Then, the modified RASBA was applied to interior detectors. It is important to note that, due to its tolerance of the striping artifacts in the perimeter, the performance of the GASBA is significantly better than that of the ASBA alone. This is attributable to its utilization of 2D-shifted frames.[24]

The GASBA was also applied to two sets of 3000-frame data sequences (referred to as Data Sets 2 and 3), obtained from an uncooled 320x240 LWIR amorphous-silicon microbolometer FPA. The raw uncorrected image frame 320 from Data Set 2 is displayed in Fig. 6.a. The resulting GASBA-corrected image is displayed in Fig. 6.b. Notice that before correction most of the image is obscured by the nonuniformity. After correction, the nonuniformity has been removed, yielding a significant increase in image clarity. The image sequence depicts an indoor scene containing a water cooler. In a similar correction for Data Set 3, Figs. 6.c and 6.d show the raw and GASBA-corrected image frame 585, which depicts a hallway scene. The quality of the NUC provided by

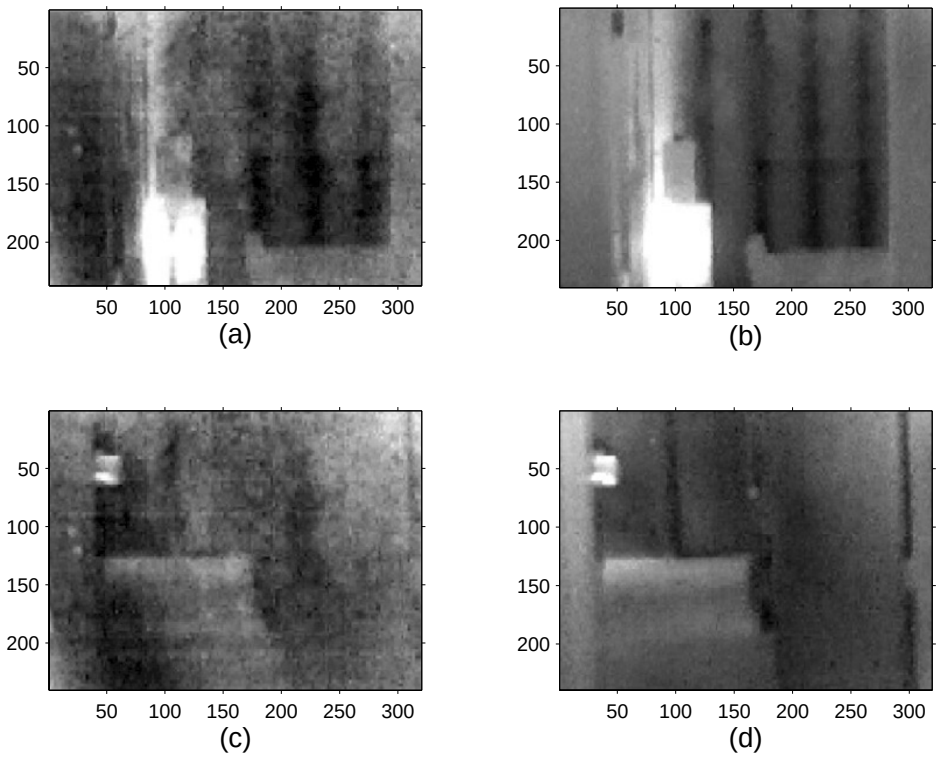

Figure 6. Imagery from Data Set 2: (a) Raw image frame 1750; (b) Image frame 1750 after correction by the GASBA. Imagery from Data Set 3: (c) Raw image frame 480; (d) Image frame 480 after correction by the GASBA. All images are statistically scaled to the same dynamic range.

the algorithm is again apparent. It is important to note that the camera used for this experiment was equipped with a mechanical shutter-based calibration system (which performs a one-point calibration). Moreover, the raw images of Fig. 6 have already been calibrated by this shutter-based system. Despite the significant level of nonuniformity present, the GASBA was capable of further improving the image quality.

A final data set was obtained from an uncooled 320x240 LWIR vanadium-oxide microbolometer FPA. Data Set 4 contains 1250 image frames, of which the raw frame 820 is depicted in Fig. 7.a. The same image frame is shown after correction by the GASBA algorithm in Fig. 7.b. This scene depicts a concrete floor with electrical test equipment at right. This camera also contained a shutter-based one-point calibration system. Notice that while most of the nonuniformity has been removed by the factory calibration system, some nonuniformity does remain and manifests as the dark, horizontal pattern in the center of the imagery. As seen in the corrected imagery, the GASBA was able to successfully remove the remaining nonuniformity, again demonstrating its high-quality correction ability.

It should be noted that the above corrections are representative of the algorithm in all cases where a video sequence is available with sufficiently diverse motion. Furthermore, it was known that the above image sequences contained a significant amount of gain nonuniformity. Despite this fact, the algorithm was able to perform well, a subject we will thoroughly investigate in future work.

4.2. Bias Compensator Convergence Study

In this subsection we perform an experiment to study how many bias compensators must be averaged to obtained reliable nonuniformity estimates. Recall that this averaging is performed in Step 6 of the algorithm description in Subsection 3.3. To perform this study, we first apply the GASBA to remove the nonuniformity in Data Set 1. Image frame 500 from this correction is displayed in Fig. 8.a. We next re-apply the GASBA to this clean

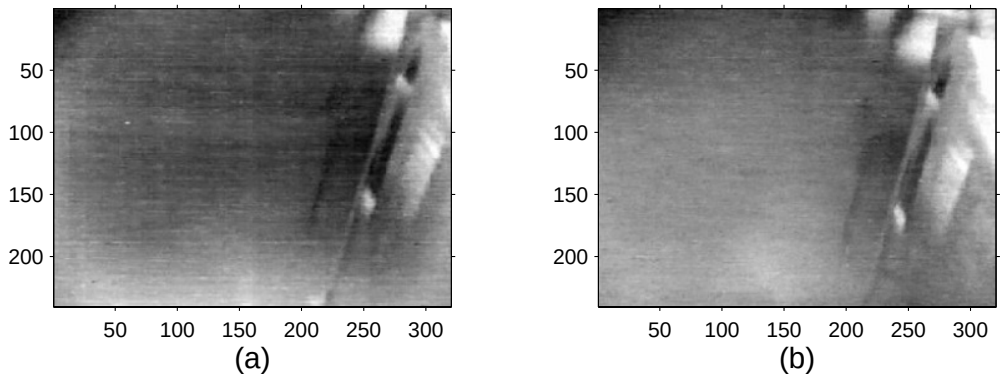

Figure 7. Imagery from Data Set 4: (a) Raw image frame 820; (b) Image frame 820 after correction by the GASBA. Both images are statistically scaled to the same dynamic range.

image sequence. Since the nonuniformity has been removed, the bias compensators produced from this second GASBA application should all be zero. Thus, any nonzero bias compensators can be attributed to error. The bias compensators produced from the image pair for frames 500 and 501 are shown in Fig. 8.b, which is linearly scaled to the full dynamic range. The shift between these image frames was $(-1.532, 0.517)$ pixels.

Of the 512 frames in the image sequence, a total of 116 image pairs exhibiting 2D motion were found. These image pairs were then used to estimate the bias compensators, each resulting in compensator estimates similar to those of Fig. 8.b. The resulting compensator estimates were then averaged for each pixel (note that due to the dynamic perimeter sizes, some detectors have less than 116 estimates). The resulting averaged bias compensator estimates are displayed in Fig. 8.c, scaled to a dynamic range of $[-0.5, 0.5]$. The range of these averaged bias compensator estimates is $[-3.12 \times 10^{-14}, 4.27 \times 10^{-14}]$, or effectively zero as expected.

Finally, to study the rate at which the compensator errors converge to zero for this data set, Fig. 8.d displays the mean absolute error and variance of the averaged bias compensator estimates as a function of the number of estimates in the average. As can be seen, the variance of the error is nearly zero after averaging just 20 estimates. After 100 estimates have been averaged, the mean absolute error and the variance are both essentially zero.

5. CONCLUSION

We have presented an overview of three recently developed algebraic scene-based nonuniformity correction algorithms. The original ASBA[21] technique is able to estimate the bias nonuniformity by using image pairs exhibiting sub-pixel one-dimensional motion. The RASBA[23] technique is able to make use of image pairs containing arbitrary two-dimensional translational motion to produce radiometrically accurate estimates of the nonuniformity. Thus, this technique is able to effectively calibrate the interior array detectors without them ever being obstructed with a calibration target. Finally, the GASBA[24] technique is able to estimate quantities that are used to compensate for bias nonuniformity by using pairs of image frames exhibiting arbitrary one- or two-dimensional global translational motion without the need for hard calibration. The key step of the algorithm is to guarantee bias uniformity in the perimeter of each image pair using the ASBA technique.

The algorithms' ability to provide high-quality NUC on real infrared data, obtained from both cryogenically cooled and uncooled FPAs, was demonstrated despite the presence of gain nonuniformity. Moreover, the ASBA and GASBA algorithms are able to perform these corrections in a shutterless manner, i.e., without the need for a blackbody calibration target. We showed that the RASBA and GASBA techniques do not suffer from the typical striping artifacts present in ASBA corrections. It was also demonstrated that the sources of error that degrade algorithm performance can be overcome when a sufficient number of compensator estimates are averaged in time. For example, for the 512-frame data set considered, these errors converged to zero after approximately 100 compensator estimates were averaged.

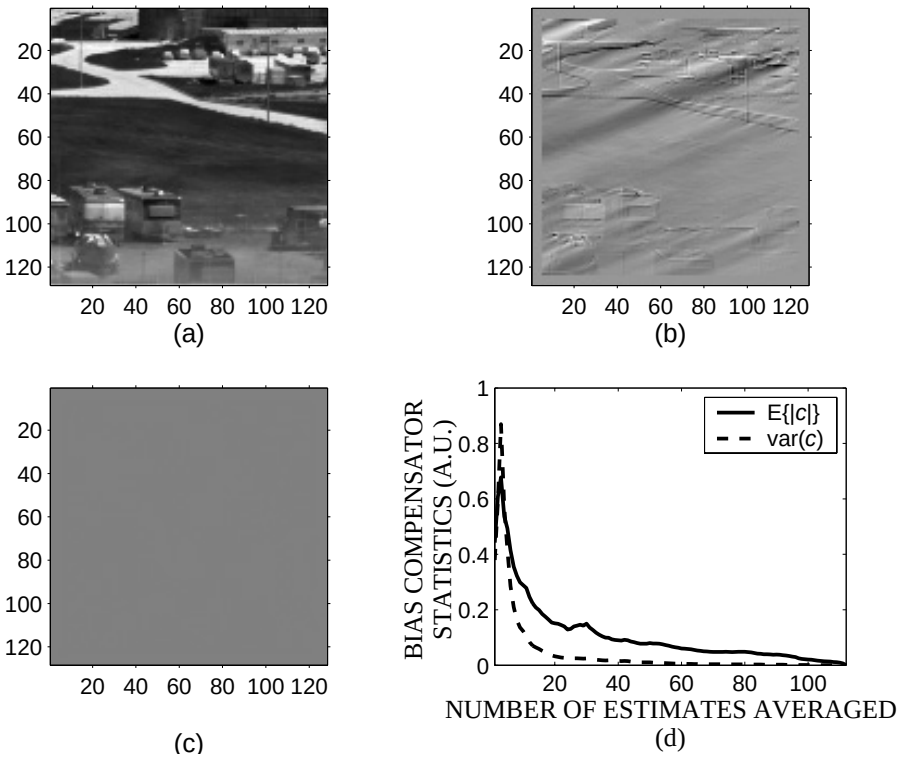

Figure 8. (a) Image frame 500 from Data Set 1 after correction by the GASBA; (b) Bias compensator estimates produced from the correction of frames 500 and 501 (linearly scaled to the full dynamic range); (c) Bias compensator estimates after averaging 116 estimate matrices; (d) Plot showing the mean and variance of the bias compensator estimates as a function of the number of estimates in the average.

One of the strengths of the algorithms is their computational efficiency, lending themselves to real-time hardware-based application. Future work will continue on the optimization of the real-time hardware implementation.

ACKNOWLEDGMENTS

The authors wish to thank Ernest Armstrong at the AFRL Sensors Directorate at Wright Patterson AFB, OH, for providing us with IR imagery. This project was partially supported by K & A Wireless, LLC, through a National Science Foundation Small Business Innovation Research (SBIR) Phase-I program (award No. 0319323).

REFERENCES

1. G. C. Holst, *CCD Arrays, Cameras, and Displays*, SPIE Optical Engineering Press, Bellingham, 1996.
2. P. M. Tribolet, P. Chorier, A. Manissadjian, P. Costa, and J.-P. Chatard, "High performance infrared detectors at Sofradir," in *Proceedings of the SPIE: Infrared Detectors and Focal Plane Arrays VI*, E. L. Dereniak and R. E. Sampson, eds., **4028**, pp. 438–456, The International Society for Optical Engineering, (Orlando, FL), July 2000.
3. A. F. Milton, F. R. Barone, and M. R. Kruer, "Influence of nonuniformity on infrared focal plane array performance," *Optical Engineering* **24**(5), pp. 855–862, 1985.
4. D. L. Perry and E. L. Dereniak, "Linear theory of nonuniformity correction in infrared staring sensors," *Optical Engineering* **32**(8), pp. 1853–1859, 1993.
5. P. M. Narendra, "Reference-free nonuniformity compensation for IR imaging arrays," in *Proceedings of the SPIE: Smart Sensors II*, **252**, pp. 10–17, The International Society for Optical Engineering, 1980.

6. P. M. Narendra and N. A. Foss, "Shutterless fixed pattern noise correction for infrared imaging arrays," in *Proceedings of the SPIE: Technical Issues in Focal Plane Development*, **282**, pp. 44–51, The International Society for Optical Engineering, 1981.
7. J. G. Harris and Y.-M. Chiang, "An analog implementation of the constant average statistics constraint for sensor calibration," in *Neural Information Processing Systems*, M. Mozer, M. I. Jordan, and T. Petsche, eds., pp. 699–705, MIT Press, (Denver, CO), 1997.
8. J. G. Harris, "Continuous-time calibration of VLSI sensors for gain and offset variations," in *Proceedings of the SPIE: Smart Focal Plane Arrays and Focal Plane Array Testing*, M. Wigdor and M. A. Massie, eds., **2474**, pp. 23–33, The International Society for Optical Engineering, May 1995.
9. Y. M. Chiang and J. G. Harris, "An analog integrated circuit for continuous-time gain and offset calibration of sensor arrays,"
10. M. M. Hayat, S. N. Torres, E. E. Armstrong, S. C. Cain, and B. J. Yasuda, "Statistical algorithm for nonuniformity correction in focal-plane arrays," *Applied Optics* **38**, pp. 772–780, Feb. 1999.
11. S. N. Torres, M. M. Hayat, E. E. Armstrong, and B. J. Yasuda, "A kalman-filtering approach for nonuniformity correction in focal plane array sensors," in *Proceedings of the SPIE: Infrared Imaging Systems: Design, Analysis, Modeling, and Testing XI*, G. C. Holst, ed., **4030**, pp. 196–205, The International Society for Optical Engineering, July 2000.
12. S. N. Torres and M. M. Hayat, "Kalman filtering for adaptive nonuniformity correction in infrared focal plane arrays," *Journal of the Optical Society of America A* **20**, pp. 470–480, Mar. 2003.
13. D. A. Scribner, K. A. Sarkady, J. T. Caulfield, M. R. Kruer, G. Katz, C. J. Gridley, and C. Herman, "Nonuniformity correction for staring focal plane arrays using scene-based techniques," in *Proceedings of the SPIE: Infrared Detectors and Focal Plane Arrays*, E. L. Dereniak and R. E. Sampson, eds., **1308**, pp. 224–233, The International Society for Optical Engineering, Sept. 1990.
14. D. A. Scribner, K. A. Sarkady, M. R. Kruer, J. T. Caulfield, J. D. Hunt, and C. Herman, "Adaptive nonuniformity correction for IR focal plane arrays using neural networks," in *Proceedings of the SPIE: Infrared Sensors: Detectors, Electronics, and Signal Processing*, T. S. Jayadev, ed., **1541**, pp. 100–109, The International Society for Optical Engineering, Nov. 1991.
15. D. A. Scribner, K. A. Sarkady, M. R. Kruer, J. T. Caulfield, J. Hunt, M. Colbert, and M. Descour, "Adaptive retina-like preprocessing for imaging detector arrays," **3**, pp. 1955–1960, IEEE International Conference on Neural Networks, (San Francisco, CA), Feb. 1993.
16. W. F. O'Neil, "Dithered scan detector compensation," in *Proceedings of the Infrared Information Symposium (IRIS) Specialty Group on Passive Sensors*, 1993.
17. W. F. O'Neil, "Experimental verification of dithered scan nonuniformity correction," in *Proceedings of the Infrared Information Symposium (IRIS) Specialty Group on Passive Sensors*, **1**, pp. 329–339, 1997.
18. R. C. Hardie, M. M. Hayat, E. E. Armstrong, and B. J. Yasuda, "Scene-based nonuniformity correction with video sequences and registration," *Applied Optics* **39**, pp. 1241–1250, Mar. 2000.
19. K. C. Hepfer, S. R. Horman, and B. Horsch, "Method and device for improved IR detection with compensations for individual detctor response." USA Patent No 5,276,319, 1994.
20. B. M. Ratliff, M. M. Hayat, and R. C. Hardie, "Algebraic scene-based nonuniformity correction in focal plane arrays," in *Proceedings of the SPIE: Infrared Imaging Systems: Design, Analysis, Modeling, and Testing XII*, G. C. Holst, ed., **4372**, pp. 114–124, The International Society for Optical Engineering, (Orlando, FL), Sept. 2001.
21. B. M. Ratliff, M. M. Hayat, and R. C. Hardie, "An algebraic algorithm for nonuniformity correction in focal plane arrays," *Journal of the Optical Society of America A* **19**, pp. 1737–1747, Sept. 2002.
22. B. M. Ratliff, "An algebraic scene-based algorithm for nonuniformity correction in focal plane arrays," master's thesis, University of Dayton, Dayton, OH, Dec. 2001.
23. B. M. Ratliff, M. M. Hayat, and J. S. Tyo, "Radiometrically accurate scene-based nonuniformity correction for array sensors," *Journal of the Optical Society of America A* **20**, pp. 1890–1899, Oct. 2003.
24. B. M. Ratliff, M. M. Hayat, and J. S. Tyo, "Generalized algebraic nonuniformity correction algorithm," *JOSA A, submitted April 2004* .

25. B. M. Ratliff, M. M. Hayat, and J. S. Tyo, "Algorithm for radiometrically accurate nonuniformity correction with arbitrary scene motion," in *Proceedings of the SPIE: Infrared Imaging Systems: Design, Analysis, Modeling, and Testing XIV*, G. C. Holst, ed., **5076**, pp. 82–91, The International Society for Optical Engineering, (Orlando, FL), Aug. 2003.
26. R. C. Hardie, K. J. Barnard, J. G. Bognar, E. E. Armstrong, and E. A. Watson, "High-resolution image reconstruction from a sequence of rotated and translated frames and its application to an infrared imaging system," *Optical Engineering* **37**(1), pp. 247–260, 1998.